RSC Advances

PAPER

View Article Online
View Journal | View Issue

Cite this: *RSC Adv.*, 2023, **13**, 36392

One-pot synthesis of unsubstituted and methyl substituted-pyrazinyl diselenides and monoselenides: structural, optical property characterization and DFT calculations†

Nisha Kushwah,*[a] Suresh M. Chopade,[a] Amey Wadawale,[a] P. Sharma[a] and G. Kedarnath *[ab]

Organoselenium compounds have long been fascinated researchers owing to their wide range of applications, such as in anticancer, in catalysis, and as molecular precursors for metal selenides. In this view, herein, the one-pot synthesis of dimethyl substituted and unsubstituted dipyrazinyl monoselenides, [(2-pyz)$_2$Se] and [(2,5-Me$_2$-3-pyz)$_2$Se], and the corresponding dipyrazinyl disenides, [(2-pyzSe)$_2$] and [(2,5-Me$_2$-3-pyzSe)$_2$], is demonstrated by the reduction of selenium metal using sodium borohydride at room temperature and a subsequent alkylation using the corresponding pyrazinyl halide in ethanol. All the diselenides and monoselenides were characterized using IR, UV-vis, photoluminescence, and NMR (^{1}H, ^{13}C{^{1}H}, and ^{77}Se{^{1}H}) spectroscopy. The molecular structures of the diselenides and monoselenides were unambiguously determined by single-crystal X-ray diffraction (SC-XRD). The optical properties, including absorption, excitation, emission, and quantum yield, of these organoselenium compounds were examined. Additionally, DFT calculations were performed to determine the HOMO and LUMO orbitals, band gap, and oscillator strength of these ligands.

Received 27th September 2023
Accepted 24th November 2023

DOI: 10.1039/d3ra06591j

rsc.li/rsc-advances

Introduction

Research in organoselenium compounds have been attracting much interest owing to their multi-faceted applications in ligand chemistry,[1] organic synthesis,[2] biochemistry,[3] materials chemistry,[4] and catalysis.[5] Furthermore, organoselenium compounds have been proved as potential candidates for technological applications in organic solar cells,[6–8] organic light-emitting diodes,[9] and p-type polymeric semiconductors.[10,11] In organic synthesis, organoselenium compounds can act as electrophiles (RSe^+Cl^-), nucleophiles (RSe^-), and radicals, leading to chemo-, regio-, and stereoselectivity under mild conditions, while in the case of materials chemistry, these compounds have been employed in the molecular precursor-driven synthesis of semiconducting metal chalcogenide nanomaterials and thin films.[12]

Moreover, it has been observed that the presence of a nitrogen atom in the aromatic ring affects the properties of these organoselenium compounds. For instance, pyridyl- and pyrazinyl-seleno groups have been demonstrated to be relatively better leaving groups compared to the phenylseleno moiety.[13] Similarly, metal selenolate precursors made up of pyridylselenolates are known to be volatile and are employed in chemical vapor deposition (CVD) for metal chalcogenide thin film deposition.[14] In addition, metal derivatives of these organoselenium compounds exhibit structural diversity. In this regard, we aimed to examine the synthesis and structural chemistry of pyrazinyl diselenides and monoselenides.

To date, a number of methods have been developed and demonstrated for the synthesis of monoselenide and diselenide compounds using elemental selenium. The methods include organometallic routes employing RLiCl or RMgBr to generate an organyl selenolate anion (RSe^-M^+) (where M = Li or Mg), followed by alkylation (Scheme 1). The most commonly used method involves the reduction of elemental selenium (Se^0) to selenide or a diselenide anion (Se^{2-} or Se_2^{2-}) depending on the molar ratio of the reactants and subsequent alkylation, yielding organyl selenols (RSeH), diorganyl selenides (RSeR), or diorganyl diselenides (RSeSeR) (Scheme 2).[15–25] Most of these reactions are quite often accompanied with the formation of selenides (R_2Se) in variable amounts, and hence the purification of diselenides is essential.

[a]*Chemistry Division, Bhabha Atomic Research Centre, Trombay, Mumbai 400 085, India. E-mail: knisha@barc.gov.in; kedar@barc.gov.in; Fax: +91-22-2550-5151; Tel: +91-22-2559-3816*

[b]*Homi Bhabha National Institute, Anushaktinagar, Mumbai 400 094, India*

† Electronic supplementary information (ESI) available: CCDC no. 2213745 for bis(2-pyrazinyl)diselenide [(2-pyzSe)$_2$] (**2**). CCDC no. 2213748 for bis(2,5-dimethyl-3-pyrazinyl)selenide [(2,5-Me$_2$-3-pyz)$_2$Se] (**3**) and CCDC no. 2213746 for bis(2,5-dimethyl-3-pyrazinyl)diselenide [(2,3-Me$_2$-3-pyzSe)$_2$] (**4**). CCDC 2213745, 2213746 and 2213748. For ESI and crystallographic data in CIF or other electronic format see DOI: https://doi.org/10.1039/d3ra06591j

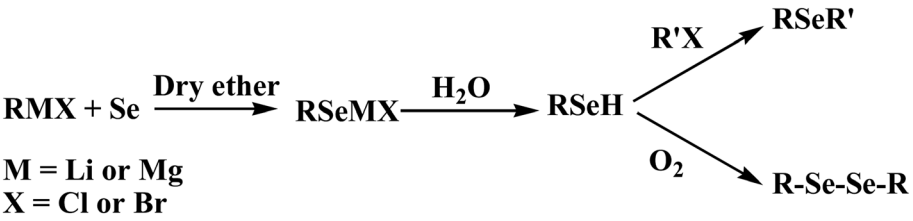

Scheme 1 Organometallic route for obtaining monoselenides and diselenides.

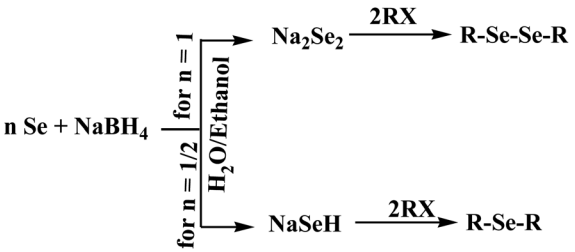

Scheme 2 Reduction route for obtaining monoselenides and diselenides.

Earlier our group reported the synthesis of various pyridyl- and pyrimidyl-selenolate ligands by adopting some of the above methods.[3,26,27] Previous experiments and observations reported that the presence of a nitrogen atom in the aromatic ring affects the properties of these organoselenium compounds. For instance, the pyridylseleno group has been demonstrated to be a relatively better leaving group compared to the phenylseleno moiety.[13] Similarly, metal selenolate precursors made up of pyridylselenolates are known to be volatile and have been employed in chemical vapor deposition (CVD) for metal chalcogenide thin film deposition.[14] In addition, the metal derivatives of these organoselenium compounds exhibit structural diversity. In view of these, we aimed to examine the synthesis and structural chemistry of pyrazinyl-diselenides and -monoselenides.

Herein, the syntheses and single-crystal X-ray structures of bis(2-pyrazinyl)diselenide [(2-pyzSe)$_2$], bis(2,5-dimethyl-3-pyrazinyl)selenide [(2,5-Me$_2$-3-pyz)$_2$Se], and bis(2,5-dimethyl-3-pyrazinyl)diselenide [(2,5-Me$_2$-3-pyzSe)$_2$] are reported. Furthermore, the optical properties, including excitation, emission, and quantum yields (QYs), of these organoselenium compounds are reported. DFT calculations were performed to find the HOMO and LUMO orbitals and the oscillator strength of these compounds.

Experimental

All the reactions were carried out under anhydrous conditions under an argon atmosphere. All reagents were purified and dried before use by standard techniques. Chloro-pyrazines (2-chloro-pyrazine and 3-chloro-2,5-dimethyl pyrazine), $NaBH_4$, and selenium metal were obtained from commercial sources. Elemental analyses were carried out on a Thermo Fisher Flash EA1112 CHNS elemental analyser. IR spectra were recorded on KBr plates on a Jasco FT-IR 6100 spectrometer. Electronic spectra were recorded on a UV-vis Jasco V-630 spectrophotometer. The ^{1}H, ^{13}C{^{1}H}, and ^{77}Se{^{1}H} NMR spectra were recorded on a Bruker Avance-II spectrometer operating at 300, 75.47, and 57.24 MHz, respectively. Chemical shifts were relative to the internal chloroform peak for ^{1}H and ^{13}C{^{1}H} NMR spectra and external Ph_2Se_2 (δ 463 ppm relative to Me_2Se) in $CDCl_3$ for the ^{77}Se{^{1}H} NMR spectra. All the luminescence measurements were carried out at room temperature using an Edinburgh Instruments FLSP 920 system, with a 450 W Xe lamp and 60 W microsecond flash lamp. The QYs were measured using an integrating sphere coated with $BaSO_4$. All the emission spectra were corrected for the detector response and excitation spectra for the lamp profile. Emission measurements were carried out with a resolution of 5 nm.

Geometry optimizations for all the ligands was carried out using the GAMESS program package. All the atoms were treated at the all-electron level and the standard def2-TZVP basis sets. The ground-state geometries of the ligands were optimized using the B3LYP hybrid density functional theory, in the gas phase as well as in the presence of $CHCl_3$ solvent. The vertical transition energies were calculated by the TDDFT methodology at the same level of theory. For the TDDFT studies, GAMESS implementation of the polarizable continuum model (PCM) was employed to account for the effects of $CHCl_3$ in all the calculations for comparison with our experimental findings, related to the absorption studies.

X-ray crystallography

The crystallographic data for bis(2-pyrazinyl)diselenide [(2-pyzSe)$_2$] (**2**), bis(2,5-dimethyl-3-pyrazinyl)selenide [(2,5-Me$_2$-3-pyz)$_2$Se] (**3**), and bis(2,5-dimethyl-3-pyrazinyl)diselenide [(2,5-Me$_2$-3-pyzSe)$_2$] (**4**) were collected using Cu K$_\alpha$ radiation (λ = 1.54184 Å) from a single crystal at 298(2) K on a XtaLAB Synergy, Dualflex, HyPix four-circle diffractometer with a micro-focus sealed X-ray tube using a mirror as a monochromator and a HyPix detector. All the data were integrated with CrysAlis PRO, and a multi-scan absorption correction using SCALE3 ABSPACK was applied.[28] The structures were solved by iterative methods using OLEX and refined by the full-matrix least-squares methods against F^2 by SHELXL-2017/1.[29,30] Hydrogen atoms were placed in idealized positions and were set riding on the respective parent atoms. All the non-hydrogen atoms were refined with anisotropic thermal parameters. The structure was refined (weighted least-squares refinement on F^2) to convergence. The crystal and structure refinement data are detailed in Table 1. All the figures were drawn using ORTEP and Mercury.[31]

Table 1 Crystallographic and structural refinement data for [(2-pyzSe)$_2$] (**2**), [(2,5-Me$_2$-3-pyz)$_2$Se] (**3**), and [(2,5-Me$_2$-3-pyzSe)$_2$] (**4**)

Formula	$C_8H_6N_4Se_2$	$C_{12}H_{14}N_4Se$	$C_{12}H_{14}N_4Se_2$
Molecular weight	316.09	293.23	372.19
Size	0.100 × 0.100 × 0.050	0.100 × 0.100 × 0.050	0.100 × 0.100 × 0.050
Crystal system	Triclinic	Orthorhombic	Monoclinic
Space group	$P\bar{1}$	$Pca2_1$	$P2_1/c$
a/Å	5.8558(6)	16.2906(2)	5.61310(10)
b/Å	6.9698(4)	6.31360(10)	5.38780(10)
c/Å	6.9700(3)	12.7839(2)	23.1681(4)
α/°	63.530(5)	90	90
β/°	87.994(8)	90	95.706(2)
γ/°	69.991(8)	90	90
V/Å^3	236.93(3)	1314.85(3)	697.18(2)
Z	1	4	2
d_{calc}/g cm^{-3}	2.215	1.481	1.773
μ (mm^{-1})/F(000)	9.461/150	3.736/592	6.535/364
θ for data collection/°	7.168 to 77.212	6.4210 to 76.8930	3.8600 to 75.6720
Limiting indices	$-5 \le h \le 7$	$-19 \le h \le 17$	$-6 \le h \le 7$
	$-8 \le k \le 8$	$-7 \le k \le 7$	$-6 \le k \le 6$
	$-8 \le l \le 8$	$-16 \le l \le 16$	$-27 \le l \le 28$
No. of unique reflns	904	2598	1381
No. of obsd reflns with $I > 2\sigma(I)$	852	2424	1283
Data/restraints/parameters	904/0/64	2598/1/160	1381/0/84
Final R_1, wR_2 indices (R_factor_gt/wR_factor_gt)	0.0394/0.1123	0.0245/0.0621	0.0280/0.0775
R_1, wR_2 (all data) (R_factor_all/wR_factor_ref)	0.0403/0.1135	0.0265/0.0637	0.0296/0.0787
Goodness of fit on F^2	1.156	1.054	1.109
Largest diff. peak and hole (e Å^{-3})	0.548 and −0.815	0.227 and −0.262	0.392 and −0.440

Crystallographic data (including the structure factors) for the structures reported in this paper have been deposited with the Cambridge Crystallographic Data Centre, CCDC no. 2213745 for bis(2-pyrazinyl)diselenide [(2-pyzSe)$_2$] (**2**). CCDC no. 2213748 for bis(2,5-dimethyl-3-pyrazinyl)selenide [(2,5-Me$_2$-3-pyz)$_2$Se] (**3**), and CCDC no. 2213746 for bis(2,5-dimethyl-3-pyrazinyl) diselenide [(2,3-Me$_2$-3-pyzSe)$_2$] (**4**).

Bis(2-pyrazinyl)selenide, [(2-pyz)$_2$Se] (1)

To a suspension of readily ground selenium powder (0.5 g, 0.63 mmol) in ethanol (50 mL), $NaBH_4$ (0.52 g, 13.7 mmol) was added in small amounts over a period under a nitrogen atmosphere with continuous stirring. Once a colorless solution of NaHSe appeared, stirring was continued for 2 h at room temperature. To this solution, chloro-pyrazine (2.9 g, 25.3 mmol) in ethanol was added dropwise with continuous stirring. After complete addition, the reaction mixture was stirred for 60 min followed by refluxing for another 2 h. The hot reaction mixture was filtered and allowed to cool to room temperature. The filtrate was dried and the crude product was extracted with hexane and filtered. The latter was recrystallized in hexane to give beige-colored crystals of monoselenide (yield: 2.4 g, 70%), mp 128–131 °C. Anal. calcd for $C_8H_6N_4Se_2$: C, 30.40; H, 1.91; N, 17.72%. Found: C, 30.65; H, 2.03; N, 17.44%. ^{1}H NMR ($CDCl_3$) δ: 8.45 (d, 2.4 Hz, 1H), 8.49 (s, 1H), 8.77 (s, 1H); $^{13}C\{^1H\}$ NMR ($CDCl_3$) δ: 142.8, 145.3, 148.3, 151.4; $^{77}Se\{^1H\}$ NMR ($CDCl_3$) δ: 472 ppm.

Bis(2-pyrazinyl)diselenide, [(2-pyzSe)$_2$] (2)

In a three-necked flask, powdered selenium metal (1.0 g, 12.66 mmol) was taken in ethanol and stirred vigorously under an argon atmosphere. To this, a small amount of $NaBH_4$ (0.48 g, 12.68 mmol) was added over a period of 30 to 45 min. Once the solution turned red, stirring was continued for an additional 2 h. Subsequently, different stoichiometric amounts of chloro-pyrazine (1.45 g, 12.66 mmol) dissolved in ethanol were added dropwise over a period of 30 min to the reaction flask depending on the synthesis of mono- and diselenides. After complete addition, the reaction mixture was stirred for 60 min followed by refluxing for another 2 h. The reaction contents were then cooled and the solvent was removed under reduced pressure. The crude product was extracted in methanol and recrystallized to get red-colored crystals of diselenide (yield: 1.3 g, 65%) mp 175–177 °C. Anal. calcd for $C_8H_6N_4Se$: C, 40.52; H, 2.55; N, 23.63%. Found: C, 40.65; H, 2.13; N, 23.44%. ^{1}H NMR ($CDCl_3$) δ: 8.35 (d, 2.4 Hz, 1H), 8.41 (s, 1H), 8.93 (s, 1H); $^{13}C\{^1H\}$ NMR ($CDCl_3$) δ: 142.2, 144.5, 145.5, 151.3; $^{77}Se\{^1H\}$ NMR ($CDCl_3$) δ: 443 ppm.

Bis(2,5-dimethyl-3-pyrazinyl)selenide, [(2,5-Me$_2$-3-pyz)$_2$Se] (3)

The preparation was a similar to that used for **1** with the exception that 3-chloro 2,5 dimethyl pyrazine (3.6 g, 25.3 mmol) was used instead of 2-chloro-pyrazine. (Yield: 2.7 g, 72%), mp 70–74 °C. Anal. calcd for $C_{12}H_{14}N_4Se$: C, 49.15; H, 4.81; N, 19.10%. Found: C, 49.00; H, 4.56; N, 19.00% ^{1}H NMR ($CDCl_3$) δ: 2.37 (s, 6H, 2-Me); 2.55 (s, 6H, 5-Me), 8.17 (s, 1H, H-6); (ring proton). $^{13}C\{^1H\}$ NMR ($CDCl_3$) δ: 20.9 (Me, C-2), 22.6 (Me, C-5), 141.1, 149.7, 151.5, 152.6. $^{77}Se\{^1H\}$ NMR ($CDCl_3$) δ: 466 ppm.

Bis(2,5-dimethyl-3-pyrazinyl)diselenide, [(2,5-Me$_2$-3-pyzSe)$_2$] (4)

The preparation was similar to that used for **2** with the exception that 3-chloro 2,5 dimethyl pyrazine (1.8 g, 12.7 mmol) was

used instead of 2-chloro-pyrazine. (Yield: 1.5 g, 64%), mp 110–112 °C. Anal. calcd for $C_{12}H_{14}N_4Se_2$: C, 38.75; H, 3.79; N, 15.05%. Found: C, 39.00; H, 3.66; N, 15.20%. ^{1}H NMR ($CDCl_3$) δ: 2.42 (s, 6H, 2-Me); 2.66 (s, 6H, 5-Me), 8.09 (s, 1H, H-6); (ring proton). $^{13}C\{^1H\}$ NMR ($CDCl_3$) δ: 20.9 (Me, C-2), 23.0 (Me, C-5), 141.2, 148.9, 149.9, 152.0. $^{77}Se\{^1H\}$ NMR ($CDCl_3$) δ: 451 ppm.

Results and discussion

Synthesis and spectroscopic analyses

The synthetic protocol of the unsubstituted and methyl substituted-pyrazinyl monoselenides and diselenides involved the generation of $NaHSe/Na_2Se_2$ through the reduction of elemental selenium dispersed in ethanol by sodium borohydride ($NaBH_4$) followed by the addition of suitable chloro-pyrazine under an inert atmosphere (Scheme 3). The addition of $NaBH_4$ to ethanolic selenium suspension, must be carried out carefully and in small amounts with vigorous stirring such that the reaction temperature did not increase beyond 40 °C. Once the solution turned red, stirring was continued for an additional 2 h. Subsequently, ethanolic chloro-pyrazine was added dropwise in stoichiometric quantities to the reaction flask followed by refluxing at 60 °C for 2 h. Later, the reaction was cooled and the crude product was processed with hexane and methanol to obtain mono- and diselenides in good yields. It may be noted that during the processing of diselenides, monoselenides in minor yields were obtained. Both the monoselenides and diselenides were further purified by recrystallization in hexane and methanol, respectively. The purity was checked by NMR.

The synthesized compounds were analytically pure and were fully characterized by different spectroscopic techniques, namely, FTIR, NMR spectroscopy (^{1}H, $^{13}C\{^1H\}$, $^{77}Se\{^1H\}$), UV-vis, luminescence, and single-crystal X-ray spectroscopy.

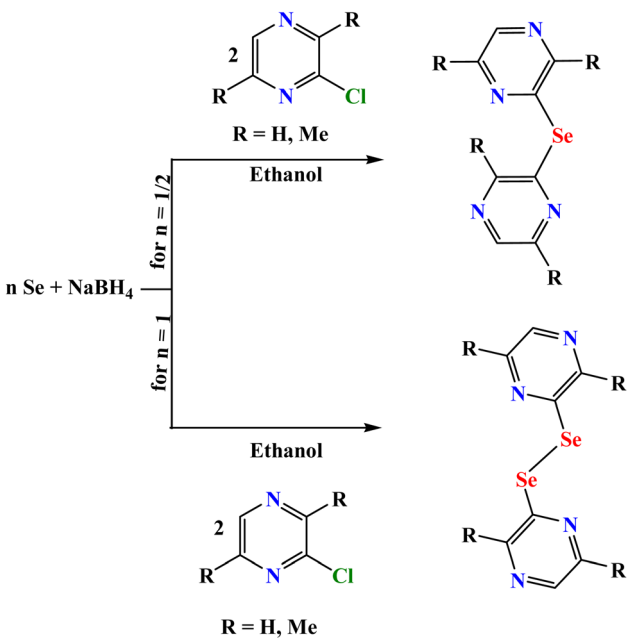

Scheme 3 Synthesis of unsubstituted and methyl substituted-pyrazinyl monoselenides and diselenides.

The IR spectra of all the selenium compounds exhibited C–Se stretching in the region 400–500 cm^{-1}. The presence of strong and sharp peaks in between 1000 and 1600 cm^{-1} could be assigned to aromatic C=C and N=C stretching vibrations of the pyrazinyl ring. The ^{1}H NMR spectra of compounds **1** and **2** showed a downfield shift of the H-3 pyrazinyl ring with respect to the starting material, 2-chloro-pyrazine. However, the shift for H-5 in the cases of **1** and **2** was negligible. For compounds **3** and **4**, the methyl protons at C-2 and C-5 were slightly deshielded compared to the methyl protons of 3-chloro-2,5-dimethyl pyrazine. The ring proton of C-6 was shifted more downfield in monoselenide **3** and nominally shifted in the diselenide **4** relative to that of the proton of 3-chloro-2,5-dimethyl pyrazine. The $^{13}C\{^1H\}$ NMR of all the compounds exhibited the expected peaks, with the ring carbons in the range of 140–153 ppm. The methyl carbon peak attached to C-2 was shifted downfield by 1–2 ppm in **3** and **4** compared to the methyl carbon of 3-chloro-2,5-dimethyl pyrazine while C-5 remained unaffected. However, the chemical shift of the C-2, C-5, and C-6 carbon peaks of **3** and **4** were downfield with respect to that of 3-chloro-2,5-dimethyl pyrazine. The $^{77}Se\{^1H\}$ NMR resonance of symmetrical diselenides appeared upfield compared to that of monoselenide. A similar trend was observed in the case of the pyrimidyl selenide ligands.[3] In the case of bis(pyrazinyl)monoselenide **1**, the ^{77}Se NMR peak appeared at 472 ppm as reported in the literature,[32] while that of bis(2-pyrazinyl)diselenide **2** emerged at 443 ppm.[33] A similar trend was seen for the $^{77}Se\{^1H\}$ NMR resonances in the methyl-substituted pyrazinyl monoselenide **3** (466 ppm) and -pyrazinyl diselenide **4** (451 ppm). The presence of the methyl group in **3** reduced the interaction between the lone pairs on selenium and π-electron system of the pyrazine ring, resulting in the shielding of the selenium nucleus of **3** compared to **1**.[3,34]

Optical properties of the ligands

The optical properties of the ligands were evaluated through UV-vis absorption spectroscopy and emission spectroscopy (Table 2) and (Fig. 1). The absorption spectrum of each ligand showed three absorption maxima (λ_{max}) as listed in Table 2. The absorption peaks clearly indicated a red-shift with the substitution of the electron-donating methyl group on the heterocyclic ring. The band gap values calculated from the λ_{onset} values clearly indicated that the HOMO–LUMO energy gap was widened with methyl substitution on the pyrazine ring. This was further confirmed by the theoretically calculated HOMO–LUMO (Fig. 1C) energy gap.

The ligands reported in the present study featured similar structures for diselenides and monoselenides but exhibited different colors in solution. The diselenides were yellow to red in color while the monoselenides were off-white. This could be ascribed to the different ligand-to-ligand charge transitions.

Luminescence properties

The excitation and emission spectra of **1**, **2**, **3**, and **4** are shown in Fig. 1B. The excitation and emission maximum of all the

Table 2 The absorption, band gap, excitation, emission, Stokes shift, and quantum yield data of the ligands in chloroform[a]

Sl no.	Compound	Absorption maximum λ (nm)	Band gap (eV) from λ_{onset} (nm)	Ex. max. λ (nm)	Em. max. λ (nm)	Stokes shift (nm)	QY (η) (%)
1	$[(2\text{-pyz})_2\text{Se}]$ (**1**)	269, 321, 362	3.56	362	400	38	1
2	$[(2\text{-pyzSe})_2]$ (**2**)	268.4, 321, 361	3.31	400	468	68	2
3	$[(2,5\text{-Me}_2\text{-3-pyz})_2\text{Se}]$ (**3**)	280.2, 317	3.58	391	436	45	2
4	$[(2,5\text{-Me}_2\text{-3-pyzSe})_2]$ (**4**)	268, 321.5, 361	3.33	399	480	80	3
5	$[(3\text{-Me-2-pySe})_2]$	313	3.26	374	435	61	1
6	$[(4,6\text{-Me}_2\text{-2-pymSe})_2]$	316	3.31	375	444	69	2.5

[a] Ex. max. = excitation maximum; Em. max. = emission maximum; QY = quantum yield.

compounds were in the ranges of 360–400 and 390–480 nm. Pyrazine has two nitrogen atoms with lone pairs of electrons and a π-deficient heterocycle. However, the compounds showed luminescence properties with Stokes shifts in the range of 30–80 nm. Interestingly, the Stokes shift for the diselenides was larger than for the monoselenides. The excitation and emission maxima of the methyl-substituted pyrazinyl monoselenide **3** was red-shifted with respect to that of the excitation and emission maxima of the unsubstituted monoselenide **1**. The red-shift may be due to the closing of the HOMO–LUMO gap with the methyl substitution on the pyrazine ring. However, this trend was minuscular in the diselenides. The quantum yields (QYs) for these selenium compounds were in the range of 1–3%. The former values for diselenides were larger than for the monoselenides due to the planar structures of the diselenides compared to the monoselenides as indicated by the torsional angles around C1–Se1–Se1–C1. The torsional angle for C1–Se1–Se1–C1 was 180° for both **2** and **4**. Furthermore, an optical property comparison of the pyrazinyl diselenides with methyl-substituted pyridyl diselenide, $[(3\text{-Me-2-pySe})_2]$ and dimethyl-substituted pyrimidyl diselenide, $[(4,6\text{-Me}_2\text{-2-pymSe})_2]$ is presented in Table 2. The results listed in Table 2 indicate that the emission maxima of the methyl-substituted pyridyl- and pyrimidyl diselenides were blue-shifted by 33–45 nm relative to the pyrazinyl diselenides; while, the quantum yields of the former ligands were comparatively lower than the pyrazinyl diselenides. The lower QY of $[(3\text{-Me-2-pySe})_2]$ with respect to $[(2,5\text{-Me}_2\text{-3-pyzSe})_2]$ may be attributed to its twisted (non-planar) structure, whereas the relatively lesser QY of planar $[(4,6\text{-Me}_2\text{-2-pymSe})_2]$ in comparison with planar $[(2,5\text{-Me}_2\text{-3-pyzSe})_2]$ may

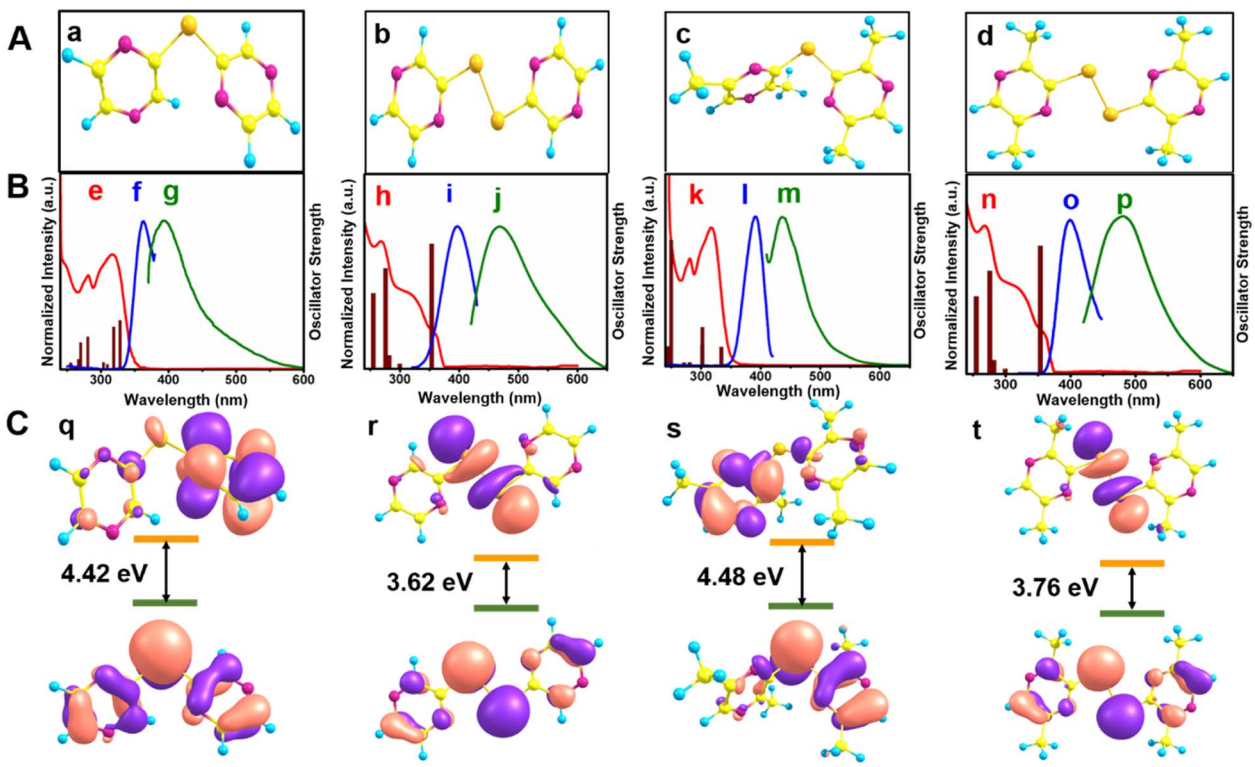

Fig. 1 (A) Optimized molecular structures (a–d); (B) absorption-, excitation-, emission-spectra (e–p); (C) HOMO and LUMO orbitals (q–t) of (a) $[(2\text{-pyz})_2\text{Se}]$ (**1**), (b) $[(2\text{-pyzSe})_2]$ (**2**), (c) $[(2,5\text{-Me}_2\text{-3-pyz})_2\text{Se}]$ (**3**), and (d) $[(2,5\text{-Me}_2\text{-3-pyzSe})_2]$ (**4**) (from left to right).

be ascribed to a ring effect. Overall, better optical properties in terms of the QY were observed for the methyl-substituted pyrazinyl diselenides with respect to that of the methyl-substituted pyridyl diselenide and -pyrimidyl diselenide.

Molecular structures of bis(2-pyrazinyl)diselenide, [(2-pyzSe)$_2$] (2) and bis(2,5-dimethyl-3-pyrazinyl)diselenide, [(2,5-Me$_2$-3-pyzSe)$_2$] (4)

Brown needle-shaped crystals of **2** and **4** were obtained by a slow evaporation of chloroform and dichloromethane, respectively. The molecular structures of **2** and **4** with their atom numbering scheme are given in Fig. 2 and 3, and selected bond length and angles are listed in Table 3.

The unsubstituted dipyrazinyldiselenide [(2-pyzSe)$_2$] (**2**) crystallizes as the triclinic/$P\bar{1}$ space group, whereas **4** crystallizes as the monoclinic/$P2_1/c$ space group. There are ten molecules of **4**, packed in a unit cell with eight molecules disposed at the corners and two molecules at the center. The geometry around Se in both diselenides is distorted tetrahedral (C1–Se1–Se1^i = 93.00(12)° (for **2**) and 93.11(8) (for **4**)) taking the lone pairs into account. In both these diselenides, the nitrogen atoms point toward the Se – bond of these molecules and have a "*cis–cis*" configuration, which is in contrast to (2-pySe)$_2$ (ref. 22) having "*trans–trans*" conformation.

The Se–Se bond distances for **2** (2.3483(7) Å) and **4** (2.3376(5) Å) are in accordance with Se–Se bond distance range of 2.290–2.390 Å on the Pauling scale.[35] The Se–Se bond distance in **4** is shorter than that of **2**, which may be due to the electronic effects of the methyl group leading to a slightly increased electron density on Se atoms leading to stronger Se–Se bond. On contrary, the Se–C bond distances in **2** (1.919(2) Å) and **4** (1.921(2) Å) are nearly same indicating that the Se–C bond distance is not affected by methyl substitution at the adjacent carbon. The Se–Se bond distance in **2** is longer than that reported for (2-pySe)$_2$ (2.30 Å)[36] and (2-pymSe)$_2$ (2.28 Å),[3] while the former distance in **4** is comparable to that documented for {py(Me-3,5)$_2$Se}$_2$ (2.35 Å).[37] Overall, the C–Se and Se–Se bond distances are in the range reported for the organic diselenides, *i.e.*, (1.91–1.97 Å) and (2.285–2.33 Å), respectively.[35] The C–Se–Se bond angles of 93(12)° and 93.11(8)° are similar to what reported for (3-CF$_3$-pySe)$_2$ (92°), while they are squeezed

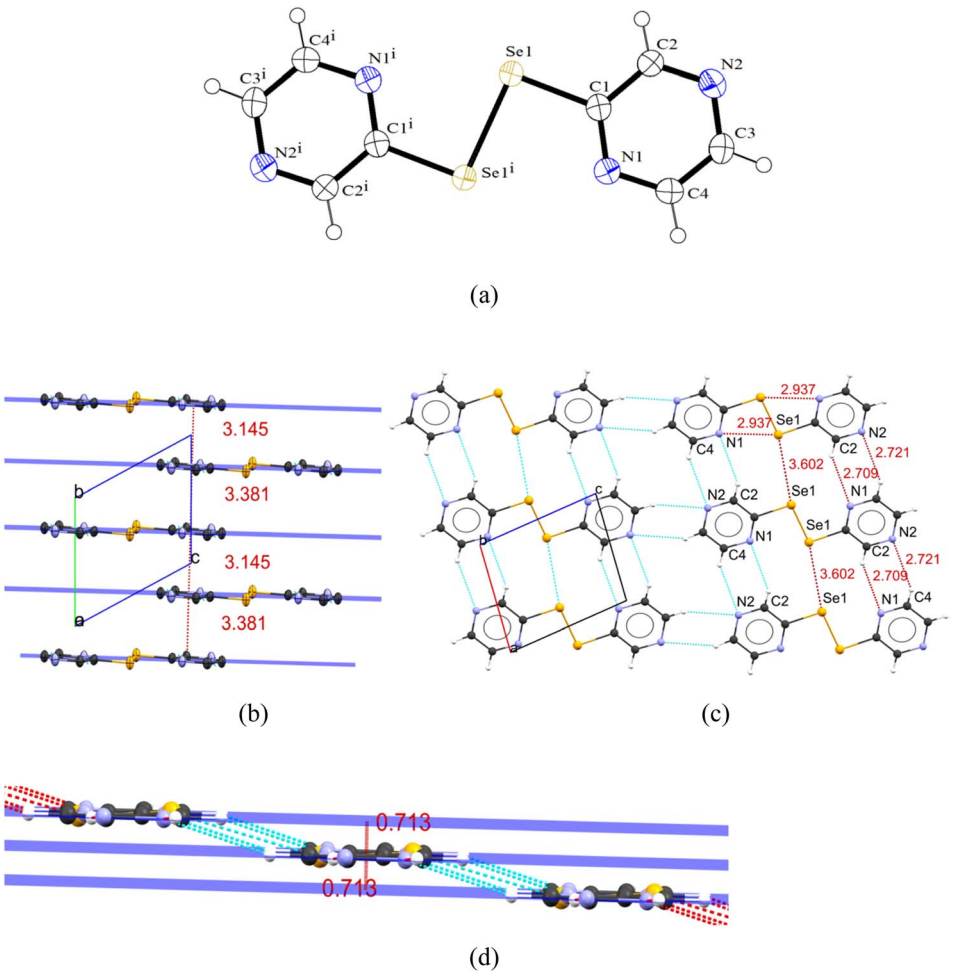

Fig. 2 (a) Molecular structure of monoclinic [(2-pyzSe)$_2$] (**2**) with an atomic number scheme (the ellipsoids are drawn with 50% probability). (b) Packing along the *b*-axis, (c) packing along the *a*-axis showing mean planes formed through interlinking of molecules, (d) molecular mean plane view along the unit cell direction ⟨1̄12⟩.

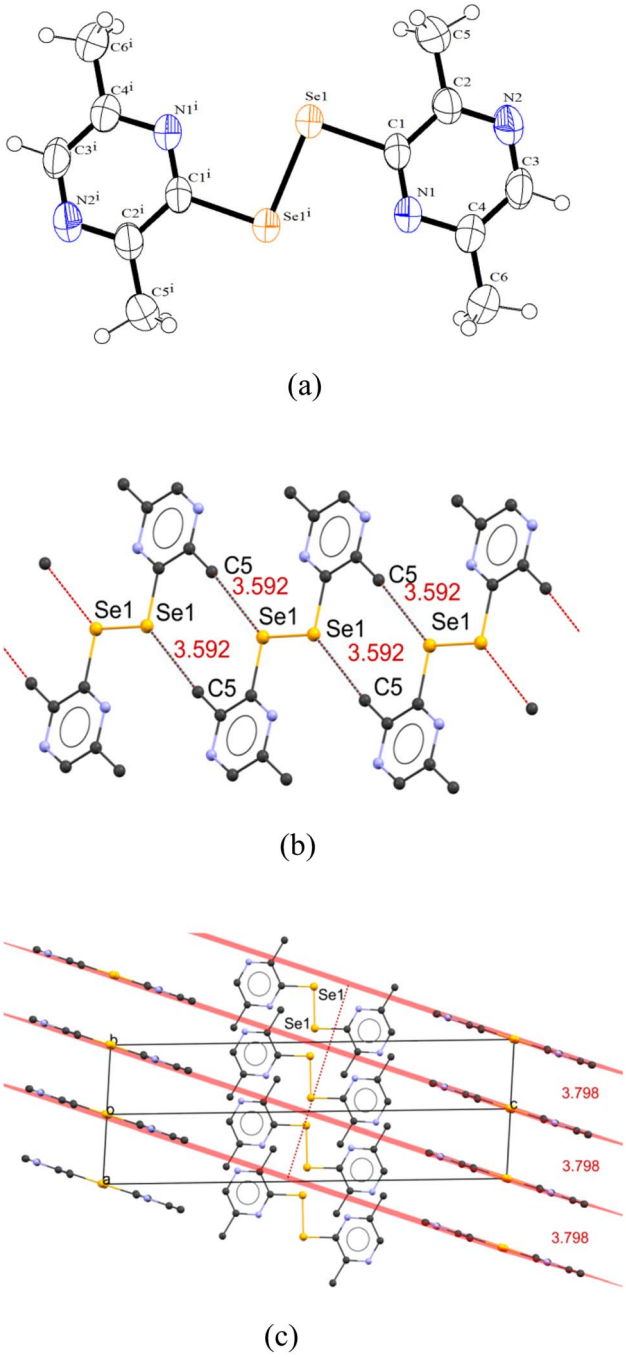

Fig. 3 (a) Molecular structure of monoclinic [(2,5-Me_2-3-pyzSe)$_2$] (**4**) with the atomic number scheme (the ellipsoids are drawn with 50% probability), (b) intermolecular interaction in **4** and (c) packing along the ⟨110⟩ unit cell direction.

compared to that documented for (5-CF_3-pySe)$_2$ (102.7°) and (2-pySe)$_2$ (104.7°).[36]

Both asymmetric units of pyrazinyldiselenides **2** and **4** are planar (torsion angle: ∠C–Se–Se–C = 180°) when compared to similar reported pyridyl ligands, *e.g.*, py_2E_2 (E = S (87.1°),[38] Se (84.3(2)°)[39] and Te (86.3(2)°),[40] (2-pymSe)$_2$ (90.2°)[3] and [$ZnCl_2$(pySe)$_2$] (98.2(2)°)).[39] The planarity suggests an extended conjugation of π electrons due to the unique positioning of the N atoms in the pyrazine ring. The planarity of pyrazinyldiselenides could be reasoned due to the secondary interactions existing between the N atom of one asymmetric unit and H–C atom of neighboring unit as explained below. Additionally, the Se⋯Se (in the case of **2**) and Se⋯C (in the case of **4**) secondary interactions between adjacent units also stabilize the two pyrazine rings in a plane.

Table 3 Selected bond lengths and bond angles for [(2-pyzSe)$_2$] (**2**) and [(2,5-Me_2-3-pyzSe)$_2$] (**4**)

	{(2-pyzSe)$_2$} (**2**)	[(2,5-Me_2-3-pyzSe)$_2$] (**4**)
Se1–Se1	2.3483(7)	2.3376(5)
Se1–C1	1.919(4)	1.921(2)
N1–C1	1.322(6)	1.322(3)
N2–C2	1.325(6)	1.325(4)
N2–C3	1.349(6)	1.339(4)
N1–C4	1.339(6)	1.343(4)
N1–C1–Se1	119.0(3)	119.11(18)
C2–C1–Se1	118.4(3)	117.8(2)
C1–Se1–Se1^i	93.00(12)	93.11(8)

The crystal packing in **2** is accomplished through short secondary contacts between a N1/N2 atom of one asymmetric unit and H2–C2/H4–C4 atom of the neighboring unit (C2–H2⋯N1 = 2.71 Å and C4–H4⋯N2 = 2.71 Å), respectively (C4–H4⋯N2 = 2.71 Å) (sum of the van der Waals radii of H and N = 2.75 Å), suggesting weak non-bonding secondary interactions between the adjacent units. The adjacent units are non-planar with the distance between the individual molecular mean planes being 0.713 Å. The mean planes of the weakly bonded molecules along the *a*-axis unit cell direction [100] are stacked along a direction perpendicular to the *a*-axis with alternating distances of 3.145 and 3.381 Å, respectively (Fig. 2b).

Owing to the presence of the methyl group, a marked difference can be observed in the crystal packing of **4** when compared to **2**. The crystal packing diagram of **4** shows the presence of intermolecular interactions between the Se1 atom of one asymmetric unit and methyl C5–H5 moiety of another unit (C5⋯Se1 = 3.592 Å) (sum of the van der Waals radii of C and Se = 3.90 Å). The nitrogen atoms do not show any short contacts as seen in **2**. The adjacent molecules are completely planar as opposed to that seen in the packing of **2**, leading to the formation of molecular planes. In 3D, two sets of stacks of planes can be seen one along the unit cell direction ⟨111⟩ and other along ⟨001⟩, arranged in an ABA fashion with an approximate distance of 3.7 Å and almost perpendicular to each other with ∼88.3° (Fig. 3).

Molecular structure of bis(2,5-dimethyl-3-pyrazinyl)selenide, [(2,5-Me_2-3-pyz)$_2$Se] (3)

Off-white-colored, needle-shaped crystals of [(2,5-Me_2-3-pyz)$_2$Se] (**3**) were obtained from the slow evaporation of monoselenide **3** in dichloromethane/hexane solution. The atomic numbering scheme and the molecular structures of **3** are given in Fig. 4, and selected bond lengths and bond angles are given in given in Table 4.

The monoselenide **3** crystallizes as orthorhombic in the $Pca2_1$-space group and adopted a 'V' shape configuration around the selenium atom with the C–Se–C angle of 99.88(15)°, which is in agreement with the similar monoselenides reported in the literature.[3,41–43] Fig. 4b shows that the molecule **3** adopts a twisted configuration, where the nitrogen atoms of two pyrazine rings do not face each other. The configuration of the molecule seems to be driven by the steric demand of the aromatic rings and the lone pair of one Se atom. The dihedral angle between the two pyrazine rings is 63.25°.

In this monoselenide, the nitrogen atoms of the pyrazine ring are "*cis–trans*" with respect to the C–Se–C bond of this molecule, which is in contrast to the pyridine nitrogen disposition relative to the C–Se–C of bis(3-methyl-2-pyridyl)selenide.[44] The average C–Se bond distance in **3** (1.929 Å) is comparable to that reported for bis(3-methyl-2-pyridyl)selenide (1.934 Å)[44] and shorter relative to that documented for $(2\text{-pymSe})_2$ (1.92 Å).[3] The C–Se bond distances are in the range reported for organic diselenides (1.91–1.97 Å).[45]

The crystal packing diagram of **3** (Fig. 4b) shows that the three adjacent asymmetric units of **3** in the 3*D* space are held together with short secondary contacts between a N and the C atoms of one asymmetric unit and H–C atom of neighboring units. For instance, N1 of pyrazine ring A lies at a distance of 2.993 Å from carbon C7 of the pyrazine ring B within the molecule. The distance is shorter than the sum of their van der Waals radii, *i.e.*, 3.25 Å, suggesting a short intramolecular interaction between the two atoms. However, the N2 atom in ring A does not participate in any interaction further. Both N3 and N4 or ring B are involved in weak secondary intermolecular bonding interactions with adjacent molecules, namely (C3–H3···N4 = 2.68 Å) and (C6–H6A···N3 = 2.62 Å) (sum of the van der Waals radii of H and N = 2.75 Å). The asymmetric units in different layers of the packing are arranged in an ABA fashion.

Table 4 Selected bond lengths (Å) and bond angles (°) for $[(2,5\text{-Me}_2\text{-}3\text{-pyz})_2\text{Se}]$ (**3**)

C1–Se7	1.931(3)	C7–Se7	1.926(4)
C1–N1	1.324(5)	C2–N2	1.325(5)
C3–N2	1.329(7)	C4–N1	1.348(5)
C7–N3	1.331(4)	C8–N4	1.330(5)
C9–N4	1.328(5)	C10–N3	1.327(5)
N1–C1–Se7	118.3(3)	C2–C1–Se7	118.1(3)
N3–C7–Se7	113.8(2)	C8–C7–Se7	123.3(3)
C7–Se7–C1	99.88(15)		

The asymmetric units in different layers interact through strong C–H···C type contacts.

Non-covalent interactions are well known for influencing the conformation and crystal structure of chalcogens. Hence it was pertinent to investigate the role of the intramolecular and intermolecular weak interactions in controlling the geometries of these ligands. Accordingly, the non-covalent interaction (NCI) method was used for characterization of the intramolecular interactions of the ligand and for evaluation of their nature. The NCI method is based on study of the reduced density gradient (RDG), which visualizes the spatial interactions. For the optimized geometries of the ligand, NCI analysis was carried out using Multiwfn software[46] and the 3D isosurfaces were visualized in VMD software.[47] The NCI analyses were carried out for an isosurface value of 0.5. The 2D RDG scatter plots and the 3D isosurface are displayed in Fig. 5. The color-filled 3D RDG isosurface depicts different types of interactions. Based on the colors, the nature of the non-covalent interactions in the 3D isosurfaces can be differentiated: weak van der Waals interactions are primarily indicated by green, while blue represents strong interactions, like hydrogen bonds. On the other hand, the red depicts steric repulsion. Similarly, in

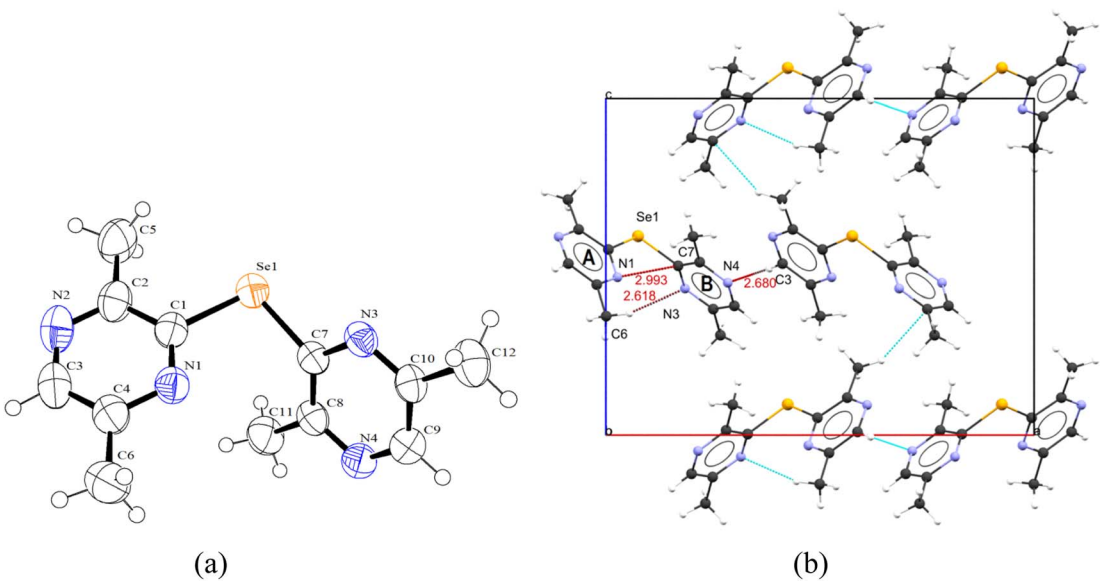

Fig. 4 (a) Molecular structure of monoclinic $[(2,5\text{-Me}_2\text{-}3\text{-pyz})_2\text{Se}]$ (**3**) with the atomic number scheme (the ellipsoids are drawn with 50% probability); (b) packing along the *b*-axis showing the intermolecular interaction in **3**.

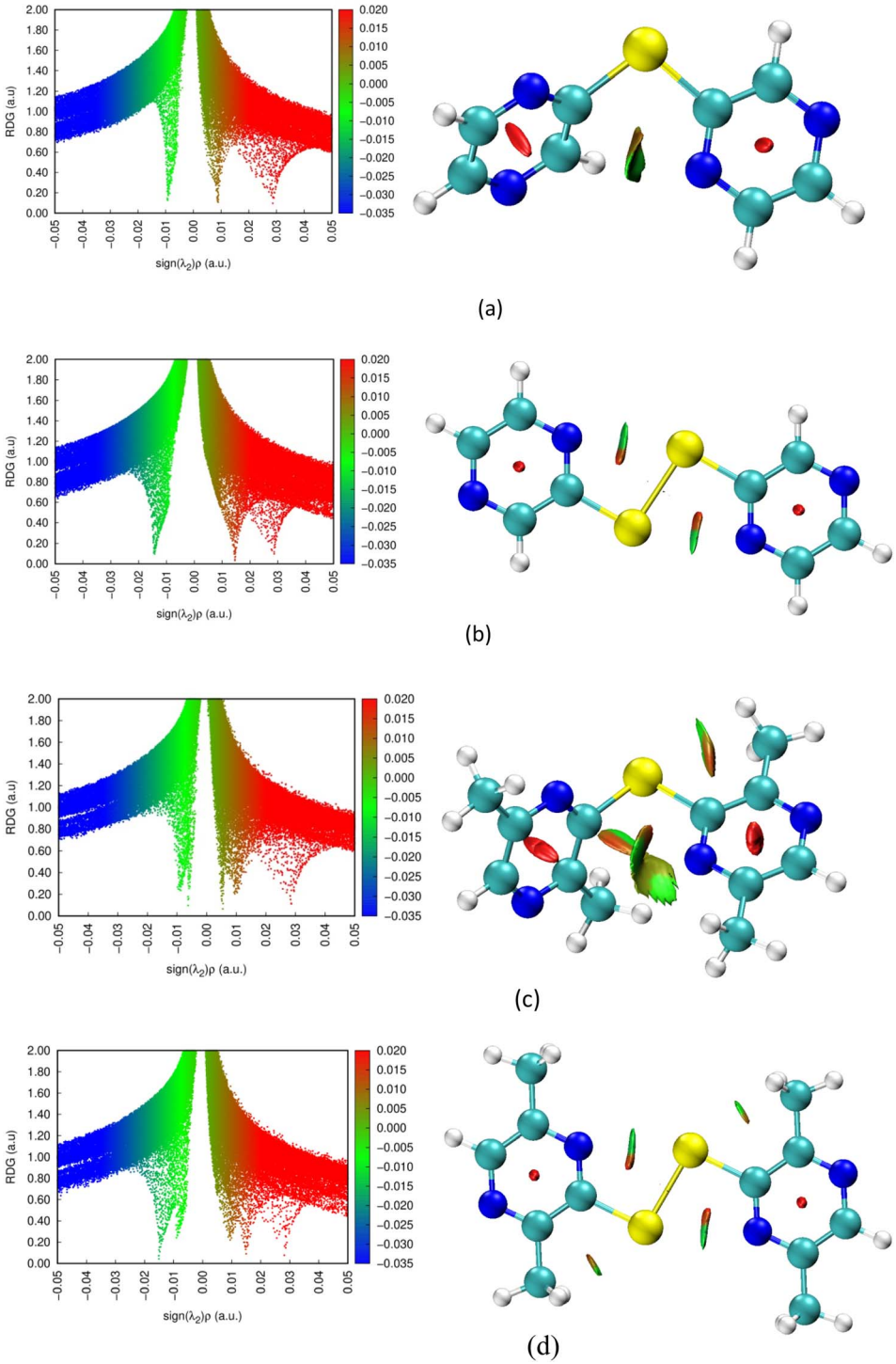

Fig. 5 NCI 2D-RDG scatter plots (left) and 3D isosurfaces (right) for (a) [(2-pyz)$_2$Se] (**1**), (b) [(2-pyzSe)$_2$] (**2**), (c) [(2,5-Me$_2$-3-pyz)$_2$Se] (**3**), and (d) [(2,5-Me$_2$-3-pyzSe)$_2$] (**4**). Blue represents strong attractive interactions, green indicates van der Waals interactions, and red indicates repulsive/steric interactions (colors online).

2D-RDG scatter plots, different types of weak interactions are represented by spikes. The blue region depicts strong attractive interactions corresponding to the strong hydrogen bonds, while the green region represents weak van der Waals interactions, and the red region corresponds to repulsive (steric effect) interactions. Based on the NCI analysis, for both diselenide ligands, the green-light brown patch between the Se–N interaction region in the 3D isosurface represents intramolecular weak non-covalent interactions, which has been ascribed to the Se⋯N chalcogen bond arising from orbital interaction between the nitrogen lone-pair of dipyrazinyl (and dimethyldipyrazinyl) and the low-lying antibonding orbital (σ*) of the selenium

moiety. This interaction leads to planarization of the diselenide ligands (Fig. 5b and d).[48] Also based on 2D scatter plots the non-covalent interaction are slightly stronger for the [(2,5-Me_2-3-pyzSe)$_2$] ligand. The red spindle-shaped area in the dipyrazinyl ring on the 3D RDG isosurface and corresponding red spike in the scatter plot indicate the steric effect in the ring. On the contrary, for monoselenides, no such intramolecular Se···N interaction could be visualized and a van der Waals interaction between the two dipyrazinyl rings was observed. However, the latter interaction was more prominent for the methyl-substituted ligand, resulting in a decrease in the C–Se–C bond angle from 102° for [(2-pyz)$_2$Se] to 99.3° for the [(2,5-Me_2-3-pyz)$_2$Se] ligand.

Conclusion

A facile synthesis of dimethyl-substituted and unsubstituted selenopyrazine compounds, namely bis(2-pyrazinyl)selenide, bis(2-pyrazinyl)diselenide, bis(2,5-dimethyl-3-pyrazinyl) selenide, and bis(2,5-dimethyl-3-pyrazinyl)diselenide, was demonstrated at room temperature by reducing elemental selenium by sodium borohydride followed by alkylation using the corresponding pyrazyl halide in ethanol. The compounds were characterized by employing various spectroscopic techniques, while their molecular structures were determined unambiguously by SC-XRD. Interestingly, the diselenides were found to be planar compared to the monoselenides, which may be due to the secondary interactions existing between the N atom of one asymmetric unit and H–C atom of the neighboring unit combined with Se···Se and Se···C secondary interactions between adjacent units. These organoselenium compounds were luminescent in nature. The studies demonstrated that the emission maximum of the methyl-substituted pyrazinyl monoselenide/diselenide was red-shifted with respect to that of the unsubstituted monoselenide/diselenide due to the narrowing of the HOMO–LUMO gap with the methyl substitution on the pyrazine ring. DFT calculations were executed to determine the HOMO and LUMO orbitals, band gap, and oscillator strength of these ligands. The planar diselenides exhibited relatively better QYs compared to the twisted monoselenides. Among the planar structures, the ring effect and substituted groups on the ring also played important roles in determining the QYs of the organoselenium compounds. Further these compounds are anticipated to act as suitable candidates in coordination chemistry and materials chemistry for the preparation of applicative metal chalcogenides by employing their metal derivatives as single-source molecular precursors.

Conflicts of interest

The authors declare no conflicts of interest.

Acknowledgements

We thank Dr A. K. Tyagi, Director, Chemistry Group, Bhabha Atomic Research Centre for the encouragement of this work.

References

1 *Organic Selenium Compounds: Their Chemistry and Biology*, ed. D. L. Klayman and W. H. H. Günther, John Wiley & Sons Inc., Chichester, 1973.
2 (*a*) A. Krief, Selenium, in *Comprehensive Organometallic Chemistry-II*, ed. E. W. Abel, F. G. A. Stone and G. Wilkinson, Elsevier, Oxford, 1995, vol. 11, pp. 515–569; (*b*) T. Wirth, Selenium, in *Comprehensive Organometallic Chemistry-III*, ed. P. Knochel, R. H. Crabtree and D. M. P. Mingos, Elsevier, Oxford, 2007, vol. 9, pp. 457–499.
3 A. S. Hodage, C. P. Prabhu, P. P. Phadnis, A. Wadawale, K. I. Priyadarsini and V. K. Jain, *J. Organomet. Chem.*, 2012, **720**, 19.
4 K. Gotluru and V. K. Jain, *New J. Chem.*, 2023, **47**, 20688.
5 C. Santi and T. Wirth, *Tetrahedron: Asymmetry*, 1999, **10**, 1019.
6 D. Meng, D. Sun, C. Zhong, T. Liu, B. Fan, L. Huo, Y. Li, W. Jiang, H. Choi, T. Kim, J. Y. Kim, Y. Sun, Z. Wang and A. J. Heeger, *J. Am. Chem. Soc.*, 2016, **138**, 375.
7 F. Gao, Y. Cheng, Q. Yu, S. Liu, D. Shi, Y. Li and P. Wang, *Inorg. Chem.*, 2009, **48**, 2664.
8 M. Heeney, W. Zhang, D. J. Crouch, M. L. Chabinyc, S. Gordeyev, R. Hamilton, S. J. Higgins, I. McCulloch, P. J. Skabara, D. Sparrowe and S. Tierney, *Chem. Commun.*, 2007, 5061.
9 S. Yamaguchi, C. Xu and T. Okamoto, *Pure Appl. Chem.*, 2006, **78**, 721.
10 M. D. Khan, M. A. Malik and N. Revaprasadu, *Coord. Chem. Rev.*, 2019, **388**, 24.
11 J. Hollinger, D. Gao and D. S. Seferos, *Isr. J. Chem.*, 2014, **54**, 440.
12 V. K. Jain and G. Kedarnath, Applications of metal selenium/tellurium compounds in materials science, *Selenium and Tellurium Reagents: In Chemistry and Materials Science*, De Gruyter, 2019.
13 A. Toshimitsu, H. Owada, S. Uemura and M. Okano, *Tetrahedron Lett.*, 1982, **23**, 2105.
14 G. Kedarnath and V. K. Jain, *Coord. Chem. Rev.*, 2013, **257**, 1409.
15 L. Brandsma and H. E. Wijers, *Recl. Trav. Chim. Pays-Bas*, 1963, **82**, 68.
16 S. Dey, V. K. Jain, S. Chaudhury, A. Knoedler, F. Lissner and W. Kaim, *J. Chem. Soc., Dalton Trans.*, 2001, 723–728.
17 D. L. Klayman and T. S. Griffin, *J. Am. Chem. Soc.*, 1973, **95**, 197.
18 K. K. Bhasin, E. Arora and T. M. Klapoetke, *J. Organomet. Chem.*, 2011, **696**, 835.
19 A. S. Hodage, P. P. Phadnis, A. Wadawale, K. I. Priyadarsini and V. K. Jain, *Org. Biomol. Chem.*, 2011, **9**, 2992.
20 K. K. Bhasin, E. Arora, K. Kaur, S. Kang, M. Gobel, T. M. Klapoetke and S. K. Mehta, *Tetrahedron*, 2009, **65**, 247.
21 L. Syper and J. Mlochowski, *Tetrahedron*, 1988, **44**, 6119; L. B. Agenas, *Acta Chem. Scand.*, 1962, **62**, 1809.
22 K. K. Bhasin and J. Singh, *J. Organomet. Chem.*, 2002, **658**, 71.

23 J. Q. Li, W. L. Bao, P. Lue and X. J. Zhau, *Synth. Commun.*, 1991, **21**, 799.
24 J. A. Gladysz, J. L. Hornby and J. E. Garbe, *J. Org. Chem.*, 1978, **43**, 1204.
25 D. S. Margolies and R. W. Pittman, *J. Chem. Soc.*, 1957, 799–805.
26 R. K. Sharma, A. Wadawale, G. Kedarnath, D. Manna, T. K. Ghanty, B. Vishwanadh and V. K. Jain, *Dalton Trans.*, 2014, **43**, 6525.
27 G. Karmakar, A. Tyagi, A. Wadawale, G. Kedarnath, A. P. Srivastava, C. A. Betty and V. Singh, *ChemistrySelect*, 2018, **3**, 10394.
28 Rigaku Oxford Diffraction, *CrysAlis PRO*, Rigaku Oxford Diffraction, Yarnton, England, 2015.
29 O. V. Dolomanov, L. J. Bourhis, R. J. Gildea, J. A. K. Howard and H. Puschmann, OLEX2: a complete structure solution, refinement and analysis program, *J. Appl. Crystallogr.*, 2009, **42**, 229.
30 G. M. Sheldrick, Crystal structure refinement with SHELXL, *Acta Crystallogr., Sect. C: Struct. Chem.*, 2015, **71**, 3.
31 L. J. Farrugia, ORTEP-3 for Windows - a version of ORTEP-III with a Graphical User Interface (GUI), *J. Appl. Crystallogr.*, 1997, **30**, 565; C. F. Macrae, P. R. Edgington, P. McCabe, E. Pidcock, G. P. Shields, R. Taylor, M. Towler and J. van der Streek, Mercury: visualization and analysis of crystal structures, *J. Appl. Crystallogr.*, 2006, **39**, 453–457.
32 K. M. Yusuf Baig, M. Kumar and G. K. Kole, *Mater. Today: Proc.*, 2022, **68**, 13.
33 G. K. Kole, A. P. Wadawale, S. Nigam, C. Majumder and V. K. Jain, *ChemistrySelect*, 2016, **1**, 4131.
34 K. K. Bhasin, V. K. Jain, H. Kumar, S. Sharma, S. K. Mehta and J. Singh, *Synth. Commun.*, 2003, **33**(6), 977.
35 T. G. Back and P. W. Codding, *Can. J. Chem.*, 1983, **61**, 2749.
36 A. S. Pedrares, M. L. D. Carril, J. Romero, J. A. G. Vázquez and A. Sousa, *Inorg. Chim. Acta*, 2010, **363**, 1212.
37 J. S. Dhau, A. Singh and R. Dhir, *J. Organomet. Chem.*, 2011, **696**, 2008.
38 N. V. Raghvan and K. Seff, *Acta Crystallogr., Sect. B: Struct. Crystallogr. Cryst. Chem.*, 1977, **33**, 386.
39 C. O. Kienitz, C. Thone and P. G. Jones, *Inorg. Chem.*, 1996, **35**, 3990.
40 K. K. Bhasin, V. Arora, T. M. Klapötke and M. J. Crawford, *Eur. J. Inorg. Chem.*, 2004, 4781.
41 E. Arora, K. K. Bhasin, S. K. Mehta, N. Sharma, A. K. K. Bhasin, C. Jacob, V. Félix and S. Neogi, *Polyhedron*, 2014, **81**, 316.
42 A. Bhalla, Y. Nagpal, R. Kumar, S. K. Mehta, K. K. Bhasin and S. S. Bari, *J. Organomet. Chem.*, 2009, **694**, 179.
43 K. K. Bhasin, Rishu, S. Singh, H. Kumar and S. K. Mehta, *J. Organomet. Chem.*, 2010, **695**, 648.
44 J. S. Dhau, A. Singh, A. Singh, N. Sharma, P. Brandão, V. Félix, B. Singh and V. Sharma, *RSC Adv.*, 2015, **5**, 78669.
45 T. G. Back and P. W. Codding, *Can. J. Chem.*, 1983, **61**, 2749.
46 T. Lu and F. Chen, Multiwfn: a multifunctional wavefunction analyzer, *J. Comput. Chem.*, 2012, **33**, 580–592.
47 W. Humphrey, A. Dalke and K. Schulten, VMD: visual molecular dynamics, *J. Mol. Graph.*, 1996, **14**, 33–38.
48 M. Iwaoka and S. Tomoda, *J. Am. Chem. Soc.*, 1996, **118**, 8077–8084.